High speed metal forming with liquid shock waves

O.E. Kosing[1] and **B.W. Skews**[2]

(Received July 1997; Final version November 1997)

High-speed metal forming with liquid shock waves, generated non-explosively, is a new field of study. The advantage of forming with liquid shock waves in a shock tube in comparison to explosive forming is better control and increased safety. This paper presents the experimental set-up of a liquid shock tube and compares different modes of operation.

Introduction

High speed metal forming using liquid shock waves is characterised by a rapid release of energy. The potential energy stored in the driving section is transformed into the kinetic energy of an air shock wave (Air mode) or into the kinetic energy of a fast moving piston (Piston mode). With the impact of either the air shock wave or the piston on a liquid surface, the kinetic energy is transformed into hydraulic pressure and a liquid shock wave is generated. The energy associated with the hydraulic pressure is used to form the work piece. Two different operating systems, the air mode and the piston mode are discussed with respect to parameters such as burst pressure, opening time of diaphragms, piston mass, and piston velocity. For the air mode the experimental results of the shock wave pressures are compared with the results calculated by theory. For the piston mode, two different piston masses are tested over a large variety of bursting pressures. The shock wave pressure and the shock wave velocity are recorded for the different operating parameters. The impulse and the energy of the initial shock wave are computed from the pressure curve. Free forming of circular disks and cylindrical tubes is investigated. The liquid shock wave for these tests is generated in the piston mode and the results are presented with respect to the liquid shock wave pressure, energy and impulse.

Experimental set-up

The experiments are carried out in a vertical water shock tube, which has a total length of 4.5 m. The shock tube consists of a stainless steel tube with an outside diameter of 106 mm and an inner diameter of 56 mm. The inside of the tube is honed smooth. The high-pressure driver is separated from the driven section by a diaphragm.

[1]School of Mechanical Engineering, University of the Witwatersrand, Private Bag 3, Wits, 2050 South Africa

[2]School of Mechanical Engineering, University of the Witwatersrand, Johannesburg

Air mode

The experimental arrangement for the air mode is shown in Figure 1. High pressures of up to 30 MPa in the driving section are required to supply enough energy to the water column for metal forming. The air is pressurised by a Haskel High Pressure Driver. Metal disks with a machined scratch of 20% of the disks' thickness are used as diaphragms. The pressure of the air shock wave is recorded by three pressure transducers of the PCB 113 A24 series. The data are recorded by a computer oscilloscope. The pressure of the liquid shock wave is recorded by using three PCB 113 A23 pressure transducers and in this case the data are recorded with a Yokogawa DL1540 oscilloscope.

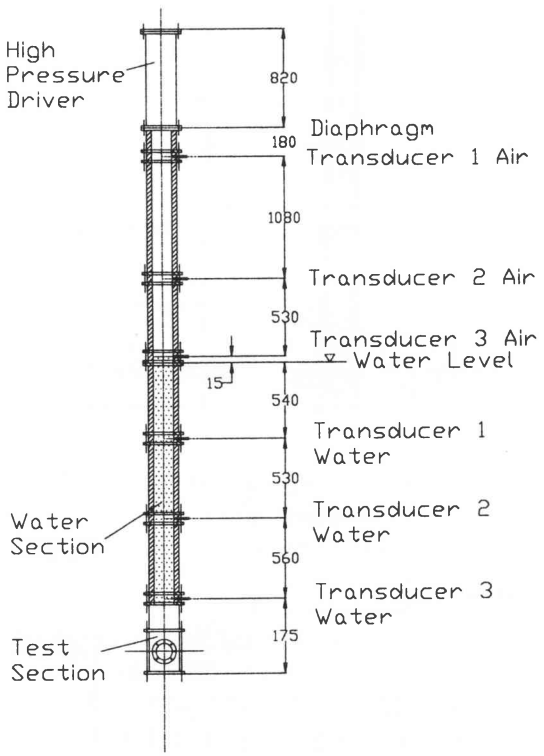

Figure 1 Schematic arrangement of liquid shock tube in air mode

Piston mode

The experimental arrangement for the piston mode is shown in Figure 2. In this case less pressure in the driving section is needed (0.3 – 3 MPa). For these low pressures a nitrogen gas bottle with an independent pressure gauge is used to supply pressurised gas. The high-pressure driver is separated from the driven section by a plastic diaphragm

which can be punctured by a needle system. The driven section is evacuated down to a pressure of approximately 5 kPa to avoid significant deceleration of the piston. A second diaphragm separates the vacuum section from the water section and prevents the water from evaporating. At the end of the driven section above the second diaphragm a light gate system is incorporated to measure the impact velocity of the piston. The data from the light gates are recorded by the computer oscilloscope. To measure the liquid shock wave, the same set-up is used as for the air mode.

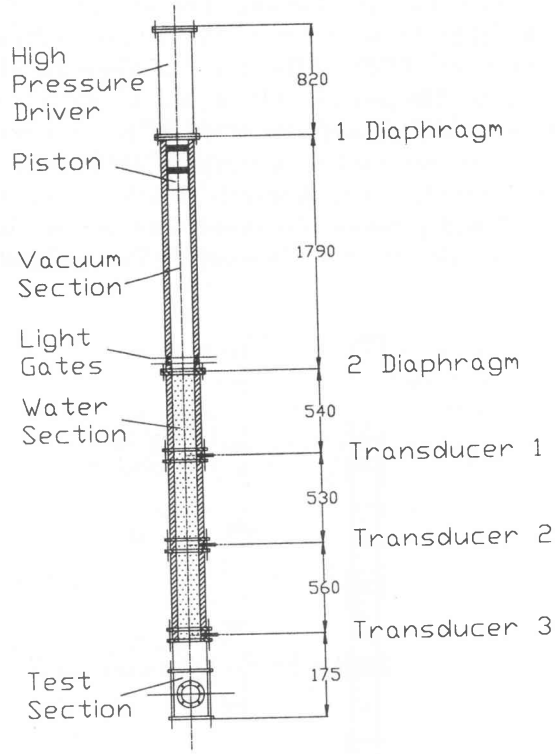

Figure 2 Schematic arrangement of liquid shock tube in piston mode

The test section

The test section is situated at the bottom of the tube and allows both the testing of circular flat disks and cylindrical thin tubes. The design of the test section allows forming into dies as well as free forming. In Figure 3 a schematic drawing shows the set-up of the test section for free forming of circular disks. The test specimen is fitted to the water section by means of an adapter. An O-ring prevents water from leaking into the test section. The die is situated under the disk and the air inside the die is evacuated through the vacuum line to prevent the deforming metal from being cushioned. The set-up of the test section for cylindrical tubes is shown in Figure 4. The liquid shock wave is focused through the nozzle into the inside of the tube. The tube is fixed in the test section by means of a bottom and top tube holder. Both tube holders contain O-rings to seal the inside of the die. The die itself is split into four parts to allow a dismantling of the die after the tube has been deformed. The inside of the die is also evacuated through the vacuum line.

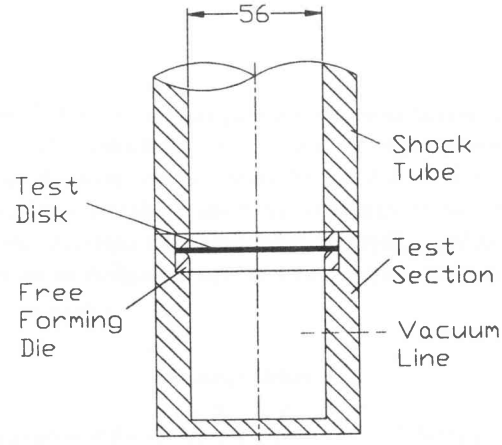

Figure 3 Schematic arrangement of test section for circular plates

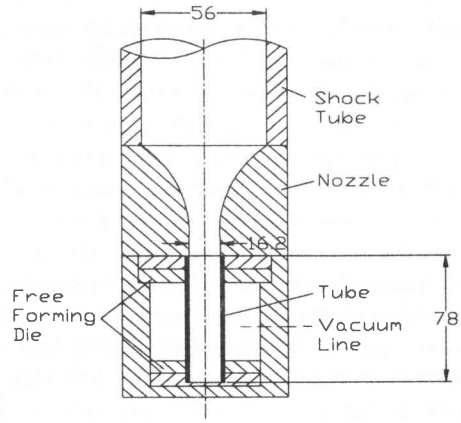

Figure 4 Schematic arrangement of test section for cylindrical tubes

Results of air mode

The air shock wave in the driven section is generated by the bursting of the diaphragm that separates the two sections. The pressure of the air shock wave can be calculated by iterating the following equation given by Mueller:[4]

$$p_4 = p_2 \left[1 - \frac{(\gamma_4 - 1)\,\frac{a_1}{a_4}\,(p_2 - 1)}{\sqrt{2\gamma_1\,(\gamma_1 - 1)\left(p_2 + \frac{\gamma_1 - 1}{\gamma_1 + 1}\right)}} \right]^{\frac{-2\gamma_4}{\gamma_4 - 1}}$$

In this equation subscript 4 stands for the conditions in the driving section and subscript 2 for the conditions behind the air shock wave. Subscript 1 describes the condition in the driven section before the shock wave. For air or

nitrogen γ is 1.4. After the air shock wave impacts on the water surface it is reflected with the pressure p_5. The pressure on the interface between the air and the water is equal and therefore the same pressure p_5 is transmitted into the water. Since the speed of sound and the density of water are much higher than in air the reflection is similar to a reflection on a solid wall. The pressure of the liquid shock wave generated by an air shock wave can be calculated using the following equation:[4]

$$p_5 = p_2 \frac{1 - \gamma + p_2 (3\gamma - 1)}{1 + \gamma + p_2 (\gamma - 1)}$$

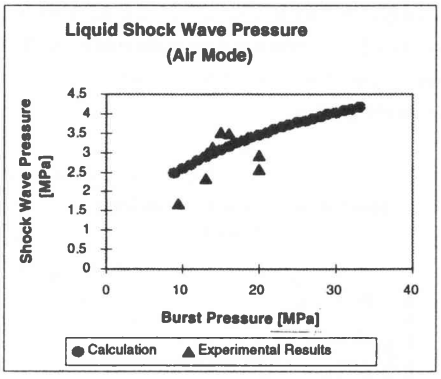

Figure 5 Liquid shock wave pressure versus burst pressure in driving section

The results of the calculations of the pressure of the liquid shock wave in comparison to experimental measurements are shown in Figure 5. The comparison shows that the experimental results are in reasonable agreement with the theoretical curve. This variability is due to the metal diaphragms opening slowly. The opening time has a great influence on the shock wave strength and the experiments have shown that it is difficult to accurately control the strength of the air shock wave. An air shock wave is characterised by a pressure jump Δp over a very short time. Behind the pressure jump the pressure stays constant (p_2 = const) for a certain amount of time (depending on the size of the driving section). This pressure history of the air shock wave determines the pressure profile of the liquid shock wave. With the impact of the air shock wave the liquid shock wave is generated. Due to the constant pressure behind the reflected air shock wave, the interface remains pressurised and the pressure behind the liquid shock wave stays constant as well. A typical wave diagram for a liquid shock wave generated with an air shock wave can be seen in Figure 6. The pressure traces of the three transducers show the liquid shock wave travelling down the shock tube. At the third transducer near the bottom wall the pressure reaches nearly double the pressure of the initial shock wave due to the reflection at the end wall. The reflected shock wave travels up the shock tube and superimposes with the initial wave. At the water surface the reflected liquid shock wave reflects as an expansion wave due to the density difference between water and air. This expansion wave, which is travelling down the shock tube, can be seen as a pressure drop in Figure 6.

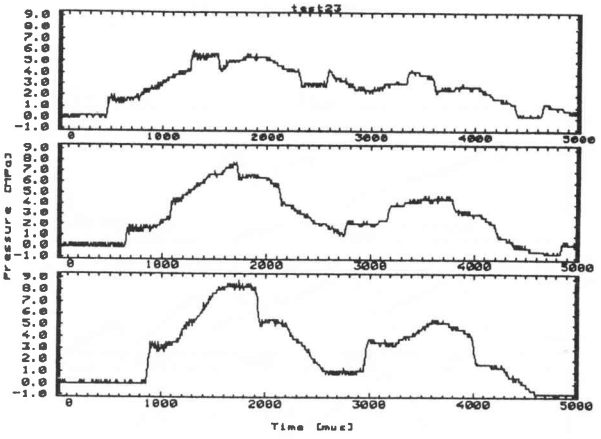

Figure 6 Pressure history for a liquid shock wave, generated with an air shock wave. Transducer 1, 2, and 3

Results of piston mode

In the piston mode the liquid shock wave is generated by the rapidly moving piston impacting on the water surface. With the impact of the piston on the water, the kinetic energy of the piston is converted into pressure energy in the liquid. The impacting piston pressurises and accelerates the water. During the impact process the piston is decelerated. This leads to a drop in the particle velocity in front of the piston and therefore to a pressure drop of the shock wave which results in a shock wave pressure profile similar to that of a blast wave. The operating cycle in the piston mode depends on the total amount of energy available and on the rate at which the energy is delivered. The total amount of energy is determined by the potential energy stored in the driving section. The potential energy is converted into the kinetic energy of the rapidly moving piston after the diaphragm has burst. The rate at which the energy is delivered to the water column and therefore to the test specimen is determined by the mass, the material and geometry of the piston. Theoretical considerations, to predict the total amount of energy and the rate at which the energy is delivered, are described by Kosing & Skews.[3] In Figures 7 and 8 pressure records for two liquid shock waves are shown, to demonstrate the influence of different piston masses. The first diagram (Figure 7) shows the results of a test performed with a heavy steel piston (3.65 kg) and the second diagram shows the results of a test performed with a very light plastic piston (0.1895 kg). For the test with the plastic piston an additional pressure transducer was introduced 75 mm above the test specimen. The bursting pressure in the driving section was 0.7 MPa for both tests. The steel piston impacted with a velocity of 21.5 m/s and the plastic piston at 102 m/s. The pressure profile of the liquid shock wave in both tests is similar to

that of a blast wave due to the deceleration of the piston during the impact. The two diagrams of the experiments performed with the different pistons show a large difference in the duration of the liquid shock wave. This is due to the smaller inertia of the plastic piston which results in a much faster deceleration during the impact.

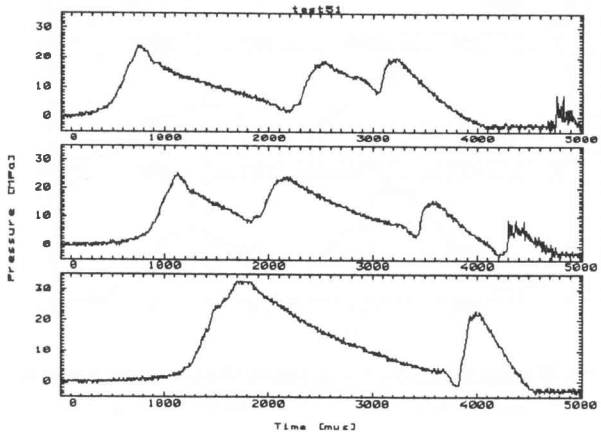

Figure 7 Pressure history for a liquid shock wave, generated with a steel piston (3.65 kg). Transducer 1, 2, and 3

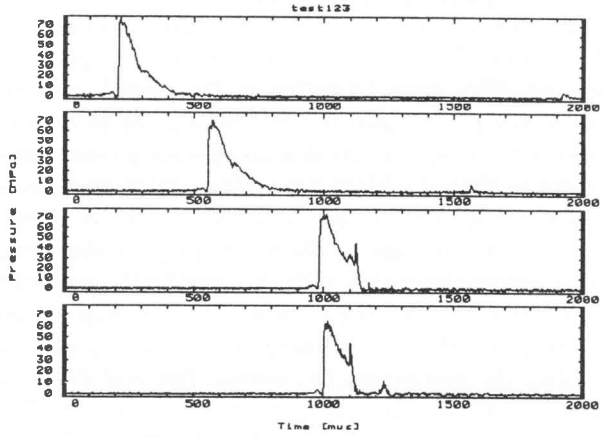

Figure 8 Pressure history for a liquid shock wave, generated with a plastic piston (0.1895 kg). Transducer 1, 2, 3, and 4

In the diagram for the light plastic piston (Figure 8) the liquid shock wave gets completely absorbed by the deforming metal in the test section. Therefore no reflected wave can be seen. For the shock wave in Figure 7 only a small part of the pressure energy is absorbed by the metal deformation and the shock wave gets reflected. The reflected shock wave travels up the shock tube and gets reflected again by the steel piston lying on the water surface. It is thus evident that the operation of the tube may be tailored to meet the particular application being considered. A comparison between the liquid shock wave generated by an air shock wave (Figure 6) and a liquid shock wave generated by an impacting piston (Figure 7 or Figure 8) clearly shows the difference between these two processes. The pressure history for the liquid shock wave generated by an air shock wave shows a constant pressure behind the initial pressure jump, which starts to increase slowly followed by a rapid increase due to the superimposition of the reflected shock wave. In comparison, the liquid shock wave generated by a piston shows an exponential pressure drop after the initial pressure jump.

In Figure 9 a comparison is made between the liquid shock wave pressures generated with the steel and the plastic pistons. The figure shows the initial liquid shock wave pressures versus the bursting pressure in the driving section. The initial liquid shock wave pressure depends on the impact velocity of the piston. A high impact velocity results in a high initial pressure jump in the water. The impact velocity of the piston depends only on its mass and therefore the curve for the plastic piston is much steeper than for the steel piston.

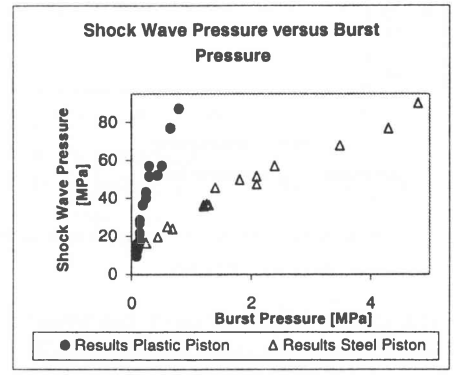

Figure 9 Shock wave pressure using steel and plastic pistons versus burst pressure in driving section

Energy and impulse of liquid shock waves

Due to their pressure history which is similar to that of a blast wave, liquid shock waves generated by an impacting piston give the possibility of calculating the energy and the impulse precisely.[1] Using the pressure trace from the experiment the energy and the impulse can be numerically integrated using the following equations.

For the energy of the liquid shock wave one can write:

$$E = \frac{A}{\rho_1 a_1} \int_{t_1}^{\infty} (p(t) - p_1)^2 \, dt \qquad (1)$$

The shock wave impulse can be calculated using:

$$I = A \int_{t_1}^{\infty} p(t) \, dt \qquad (2)$$

A is the cross-sectional area, ρ is the density and a is the speed of sound. The subscript 1 refers to the conditions in front of the liquid shock wave. In Figure 10 a comparison of the shock wave energies generated with the plastic and the steel pistons can be seen. The shock wave

energy generated with the steel piston is slightly smaller than the values for the plastic piston. This is most probably due to higher friction losses when using the steel piston. The steel piston is much longer in comparison to the plastic piston and for very slow piston velocities the friction losses become more important. A comparison of the generated shock wave impulse is made in Figure 11. The shock wave impulse generated by the steel piston is much larger than for the plastic piston. In the equation for the impulse, the mass of the piston plays a much more important role than in the equation for the energy, where the mass is compensated for by the velocity, which is squared.

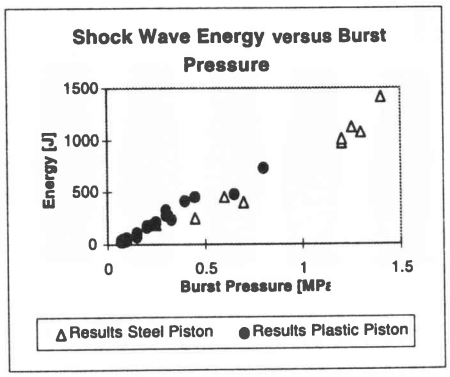

Figure 10 Shock wave energy using steel and plastic pistons versus burst pressure in driving section

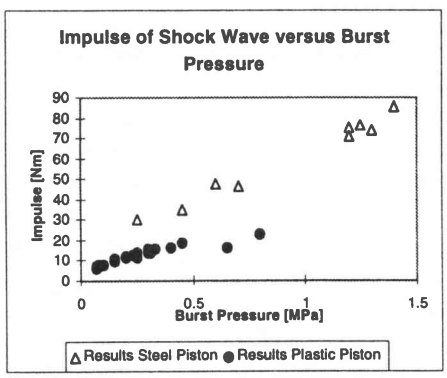

Figure 11 Shock wave impulse using steel and plastic pistons versus burst pressure in driving section

Results of metal forming

Free forming of circular metal disks

Johnson[2] proposed a guide for assessing the behaviour of metals plates subjected to impact, using a dimensionless number defined as

$$\alpha = \frac{\rho V^2}{\sigma_d} \tag{3}$$

where V is the impact velocity, ρ the material density and σ_d the damage stress. Nurick[5] suggests writing the damage number in terms of the impulse and to substitute the damage stress σ_d with the yield stress σ_o. Equation (3) can then be written as:

$$\alpha = \frac{I^2}{A_0^2 t^2 \rho \sigma_o} \tag{4}$$

To classify the high velocity deformation of plates Nurick & Martin[6] give the following table:

Table 1 Classification of high velocity deformation of circular plates

$1 * 10^{-5}$	quasi-static elastic
$1 * 10^{-3}$	plastic behaviour starts
$1 * 10^{-1}$	moderate plastic behaviour
$1 * 10^{1}$	extensive plastic behaviour
$1 * 10^{3}$	hypervelocity impact

Free forming with circular disks was performed with copper disks. The test specimen consisted of copper C106 with a thickness of 0.55 mm and 0.9 mm. The set-up of the test section for free forming of circular disks can be seen in Figure 3. For the experiments the light plastic piston (0.1895kg) was used. In Tables 2 and 3 the results of the experiments are given. The energy and the impulse were numerically integrated using equations (1) and (2), respectively, and Johnson's damage number was calculated with the modified equation (4). The maximum deformation D is the midpoint deflection of the deformed disk.

For the free forming tests, Johnson's damage number α lies in the range of extensive plastic behaviour (see Table 1). The results show that the damage number is not necessarily increasing with increasing deformation. For example, in Table 2 the damage number decreases from 11.5 to 11.0 for an increasing deformation (14.4 mm to 16.15 mm). A similar decrease in the damage number can be seen in Table 3. Therefore it appears that the damage number, and with it the impulse of the shock wave, is not really adequate for classifying the deformation process of metal disks. The deformation process of the disk seems to be more dependent on the shock wave energy which increases monotonically with increasing deformation. Attempts to classify the deformation process should therefore be made with respect to the shock wave energy.

Table 2 Results of free forming tests with 0.55 mm copper disks

D [mm]	P [MPa]	E [J]	I [Ns]	α
10.95	13.96	45.88	7.93	16.68
13.45	19.62	79.25	9.75	25.2
14.4	19.32	90.3	11.5	35.08
16.15	25.70	116.96	11.0	32.1

Table 3 Results of free forming tests with 0.9 mm copper disks

D [mm]	P [MPa]	E [J]	I [Ns]	α
16.03	37.25	144.3	9.94	9.71
17.22	42.26	184.9	11.2	12.43
17.5	43.2	183.5	11.17	12.36
19.0	51.9	219.6	11.12	12.2

In Figures 12 and 13 pictures of the deformed disks are shown. The maximum midpoint deformation increases from the left to the right hand side.

Figure 12 Pictures of deformed copper disks. Thickness 0.55 mm. From left to right: 10.95, 13.45, 14.4, 16.15 mm midpoint deflection

Figure 13 Pictures of deformed copper disks. Thickness 0.9 mm. From left to right: 16.03, 17.22, 17.5, 19.0 mm midpoint deflection

Free forming of cylindrical metal tubes

Free forming of cylindrical tubes was performed with test specimens of mild steel (ANSI B. 93. 4M. 81) and out of copper (C106). For the mild steel specimens the steel piston, with a mass of 3.665 kg, and for the copper specimens an aluminium piston, with a mass of 0.87 kg, was used. The set-up of the test section is shown in Figure 4. The results of the tests with the steel tubes can be seen in Table 4 and the results for the copper tubes in Table 5. Pictures of the deformed tubes are shown in Figures 14 and 15. The results show that after an initial deformation over the whole length of the tube (see Figure15, first tube), the deformation at the top part lags behind the deformation of the bottom part. This leads to the final shape of the tubes, which is more bulged towards the bottom. The steel tubes show a symmetrical behaviour about the longitudinal axis whereas the copper tubes are sometimes unsymmetrical, which is most probably due to irregular wall thickness.

Table 4 Results of free forming tests with 1.6 mm steel tubes

Dia [mm]	P [MPa]	E [J]	I [Ns]
24.1	43.4	1995.5	101.8
26.0	53.04	2373.6	114.0
torn	50.46	2586.33	123.89

Table 5 Results of free forming tests with 1.4 mm copper tubes

Dia [mm]	P [MPa]	E [J]	I [Ns]
21.4	35.5	401.3	24.1
24.7	42.2	435.8	28.0
25.2	47.21	554.9	34.56
25.4	46.7	532.7	34.3
26.35	45.05	569.9	34.0
26.6	50.3	649.03	37.6
torn	56.55	789.8	39.35

Figure 14 Picture of deformed mild steel tubes. From left to right: Maximum diameter [mm] 24.1, 26.0, torn

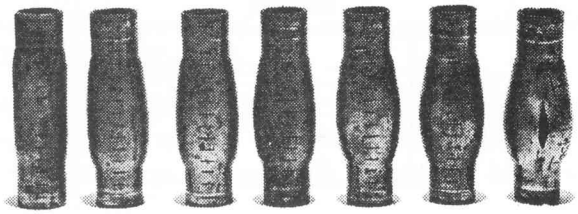

Figure 15 Picture of deformed copper tubes. From left to right: Maximum diameter [mm] 21.4, 25.2, 25.4, 26.35, 26.6, torn

Conclusions

The tests performed with the liquid shock tube in the air mode show that this process is not precisely controllable. The process depends strongly on the bursting pressure of the diaphragms and their opening times. The liquid shock wave generated in the air mode has a very long duration and gets superimposed by the remaining static pressure in the shock tube. This static pressure can be high because of the much higher initial pressure required in this mode. This makes it very difficult to determine if the whole deformation of the test specimen is caused by the initial liquid shock wave or if a part of the deformation is due to the static pressure. Also the energy and the impulse of the liquid shock wave are difficult to determine. Another aspect is the total amount of energy, which is needed in the air mode. The driving section requires a much higher pressure to generate a liquid shock wave which is sufficiently strong enough for metal forming.

The controllability of the shock tube in the piston mode is much better, as shown in the results of the piston mode. Different piston masses and materials allow the exact amount of energy required for the metal forming to be produced. The pressure history of the liquid shock wave generated in the piston mode is similar to that of a blast wave and therefore the energy and the impulse of the liquid shock wave can be precisely determined. The total amount of energy required in the driving section is much lower than for the air mode. Therefore plastic diaphragms can be used to separate the driving section from the driven

section. The plastic diaphragms allow the use of a needle system to puncture the diaphragms at the desired pressure which increases the controllability.

The comparison between the light plastic piston and the heavy steel piston (see Figures 7 and 8) shows that the duration of the liquid shock wave depends on the inertia of the piston. The maximum pressure of the liquid shock wave depends on the impact velocity and the material of the piston. With the plastic piston small portions of pressure energy over a very short interval of time can be delivered to the workpiece. The short duration of the liquid shock wave is an advantage of the light piston over the heavier steel piston as the shock wave does not get reflected. For the heavy steel piston the reflected shock wave impacts a second time on the test specimen and can cause an additional deformation. Investigations of this effect still need to be undertaken.

The results of the free forming tests with copper disks, which are presented in Tables 2 and 3, show that the deformation of the test specimens is governed by the pressure energy of the liquid shock wave. Further tests have to be performed to get more results and to work out a theoretical approach to predict the maximum deflection of metal disks.

A liquid shock wave focused into a metal tube allows the tube to expand to a greater diameter. For this deformation process a higher amount of pressure energy is required and therefore a metal piston (aluminium or steel) has to be used. The results in the free forming of cylindrical tubes show that the deformation of the tubes is not symmetrical. The bottom part gets more deformed than the top part of the tube. This leads to a final shape which is more bulged towards the bottom.

This exploratory study has shown that controlled metal deformation can be undertaken using a liquid shock tube, and that the method has potential for development as a manufacturing process, especially for the expansion of tubes. More detailed investigations are currently under way, including studies relating to metal forming into dies and detailed surface figuring.

The liquid shock tube also serves due to its good controllability as a very useful tool to further investigate the phenomenon of high speed metal forming. A new project has been started to optically investigate the metal specimens during the impact of the liquid shock wave by using a high speed video camera.

References

1. Cole RH 1965. *Underwater Explosions.* Dover Publications, Inc., New York.

2. Johnson W 1972. *Impact Strength of Materials.* Edward Arnold, p.303.

3. Kosing OE, Skews BW 1997. The use of liquid shock waves for metal forming. *Proceedings of the 21st International Symposium on Shock Waves,* Australia.

4. Mueller M 1987. *Stosswellenfokusierung in Wasser.* Dissertation, RWTH Aachen, Germany.

5. Nurick GN 1989. An empirical solution for predicting maximum central deflections of impulsively loaded plates. *Int. Conf. Mech. Prop. Materials at High Rates of Strain,* Oxford.

6. Nurick GN, Martin JB 1989. Deformation of thin plates subjected to impulsive loading – a review, Part II. *Int. J. Impact Engng,* **8**, 2, pp.171–186.